Proceedings of the ASME 2022
International Design Engineering Technical Conferences and
Computers and Information in Engineering Conference
IDETC/CIE 2022
August 14-17, 2022, St. Louis, Missouri

IDETC2022-89948

VIBRATION ENERGY HARVESTER WITH PIECEWISE LINEAR NONLINEAR OSCILLATOR AND CONTROLLABLE GAP SIZE

Jacob Veney
Nonlinear Vibrations and Dynamics Lab
Department of Mechanical and
Aerospace Engineering
The Ohio State University
Columbus, Ohio 43210
Email: veney.10@osu.edu

Kiran D'Souza*
Nonlinear Vibrations and Dynamics Lab
Department of Mechanical and
Aerospace Engineering
The Ohio State University
Columbus, Ohio 43210
Email: dsouza.60@osu.edu

ABSTRACT

Recently, vibration energy harvesting has been seen as a viable energy source to provide for our energy dependent society. Researchers have studied systems ranging from civil structures like bridges to biomechanical systems including human motion as potential sources of vibration energy. In this work, a benchtop system of a piecewise-linear (PWL) nonlinear vibration harvester is studied. A similar idealized model of the harvester was previously looked at numerically, and in this work the method is adjusted to handle physical systems to construct a realistic harvester design. With the physically realizable harvester design, the resonant frequency of the system is able to be tuned by changing the gap size between the oscillator and mechanical stopper, ensuring optimal performance over a broad frequency range. Current nonlinear harvester designs show decreased performance at certain excitation conditions, but this design overcomes these issues while also still maintaining the performance of a linear harvester at resonance. In this investigation, the system is tested at various excitation conditions and gap sizes. The computational response of the resonance behavior of the PWL system is validated against the experiments. Additionally, the electromechanical response is also validated with the experiments by comparing the output power generated from the experiments with the computational prediction.

INTRODUCTION

Vibration energy harvesting is an increasingly viable energy source for everything from individual devices to large-scale power generation. By harnessing this ubiquitous energy source in physical systems, electrical energy can be generated for a variety of applications. On small scales, vibration energy harvesters can be used to power individual electronic devices. This sustainable and plentiful energy source removes the need for external power sources, while maintaining the necessary energy density [1–3]. This technology could also be implemented in larger-scale power generation. One vast potential source of this energy is from waves on the surface of the ocean [4, 5]. With miles of coastline and constant movement, immense energy is available for power generation. It is estimated that globally, 2.11 TW of energy is available for harvesting from ocean waves, with 280 GW available in the coastal waters along the United States [6]. Due to the wide variety of possible applications, this technology has the potential to fulfill many of society's growing energy needs, while also reducing dependency on traditional carbon based fossil fuel energy sources [7].

The earliest and most basic form of vibration harvesters are based on simple lightly damped linear oscillators [8]. These devices provide maximum energy generation while operating at the device's resonant frequency, but show a dramatic decrease in performance as the frequency of ambient vibration moves away

*Address all correspondence to this author.

from resonance. This is due to the inherent frequency response characteristics of these systems. In order to broaden the effective frequency range, researchers have devised different harvesting techniques to preserve maximum efficiency while also increasing the effective frequency range. One alternative method for broadband transduction is array-harvesting [9–11], which uses many linear systems with different resonant frequencies, allowing the system to harvest relatively effectively over a predetermined range. While this method did show increased performance at the resonance values of the array, the system setup is complex and the array method reduces the energy density of the system, making implementation difficult. Another alternative method is nonlinear energy harvesting [12, 13] which introduces a nonlinearity into the system. These systems exploit the material and geometric nonlinearities to broaden the effective frequency range. While this method did show certain improvements, the performance still did not match that of linear harvesters at resonance.

Another harvesting method that researchers are currently investigating is piecewise-linear (PWL) nonlinear harvesting [14–16]. These devices introduce a nonlinearity in the form of a mechanical stopper to the conventional linear system. While it has been found that these systems broaden the effective frequency range for up-sweep excitation conditions, the performance is often reduced for arbitrary excitation conditions. These PWL harvesters also do not achieve the same performance as linear harvesters at resonance. In order to achieve maximum performance over a broad frequency range with a variety of excitation conditions, a modification of the PWL nonlinear harvester has recently been proposed and numerically investigated [17]. In this design, an adjustable mechanical stopper is introduced. By adjusting the gap size in the PWL oscillator, the resonant frequency of the harvester system is able to be tuned to match the excitation signal, achieving a continual optimized performance. In order to employ this control method, the bilinear amplitude approximation (BAA) method [18–21] is leveraged to efficiently calculate the response of PWL nonlinear systems. This method is first used to compute the optimal gap size over the interested frequency range. After extracting the external frequency and amplitude the gap size can then be adjusted to the precomputed optima position. Through a numerical investigation, it was found tha the system with the adjustable gap performed better than many current vibration harvesters since it could operate effectively fo drifting and stationary excitation conditions.

In this paper, an experimental investigation is conducte to demonstrate the effectiveness of the new PWL energy har vester with a controllable gap for the first time on a physica system. The new system is tested at different excitations con ditions where the system dynamics are monitored. These result are then compared to traditional linear designs, as well as a nu merical simulation of the proposed system. Modifications of th computational model and extensions to the method to account fo parameters not considered in the original idealized PWL oscilla tor are also presented.

The remainder of this paper is organized as follows. The methodology section first introduces the changes to the computational model. The dynamics of the system as well as the solution process are then presented. Next, the experimental setup and process used to identify system parameters is presented. Finally, the physical investigation section outlines the experimental process and compares the measured performance of the harvester to the computational model.

METHODOLOGY

This section presents the mathematical model of the PWL mechanical system and how to solve for the system dynamics using the BAA method. Next, the electromechanical model is introduced. Finally, the experimental setup is discussed and how the mechanical parameters of the system were identified is explicated.

Mathematical Model

The mechanical model that will be discussed in this section is given in Fig. 1. As mentioned in the introduction, this research is based on a numerical study of the harvester, which did not account for the mass of the stopper in the system [17]. In order to model the system more accurately, adjustments have been made to the original model and are introduced below.

The harvester consists of a mass m connected to a spring of stiffness k oscillating in a base-excited system. This mass is intermittently contacting a mechanical stopper of mass m^* and stiffness k^*. It also assumes that all the damping in the system is linear and viscous with damping coefficients given by c and c^*. By using a linear actuator, the gap size $g(t)$ between the mass and mechanical stopper can be adjusted. Note that the position of the gap size is only dependent on the actuator position, not the mass displacement. The key change to the methodology from

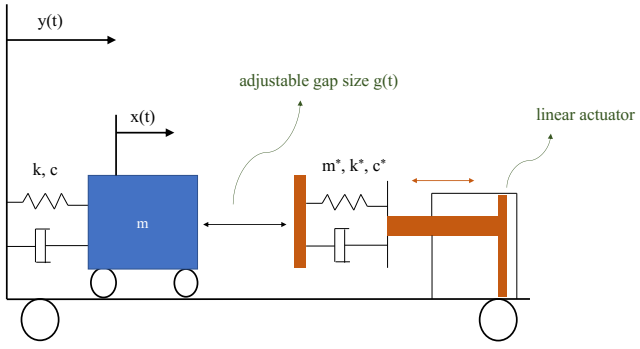

FIGURE 1: PWL harvester mechanical model.

[17] is that the mass of the spring and plate m^* that the primary mass m interacts with are now being accounted for, which will affect how the following equations and variables are defined. The base displacement of the system is assumed to be $y(t)$ and the displacement of the mass is represented by $x(t)$. The equations of motion used are in Eqn. (1).

$$\begin{aligned} \bar{m}\ddot{\bar{x}}_c(t)+(c+c^*)\dot{\bar{x}}_c(t)+(k+k^*)\bar{x}_c(t) = \\ -\bar{m}\ddot{y}(t)+c^*\dot{g}(t)+k^*g(t) \text{ when } \bar{x}\geq g, \\ m\ddot{\bar{x}}_o(t)+c\dot{\bar{x}}_o(t)+k\bar{x}_o(t) = -m\ddot{y}(t) \text{ when } \bar{x}<g. \end{aligned} \tag{1}$$

In Eqn. (1), some parameters were transformed for ease of calculations: $\bar{x}=x-y$ denotes the relative displacement between the base and mass m; the parameter $\bar{m}=m+m^*$ was also introduced to represent the combined mass of the mass and stopper in the closed state. Note that the subscript o denotes the system in the open case or $\bar{x}<g$ and the subscript c denotes the closed case or $\bar{x}\geq g$. This equation can be rewritten as

$$\begin{aligned} \ddot{\bar{x}}_c(t)+2(\zeta_{c1}\omega_{c1}+\zeta_{c2}\omega_{c2})\dot{\bar{x}}_c(t)+(\omega_{c1}^2+\omega_{c2}^2)\bar{x}(t) = \\ \ddot{y}(t)+2\zeta_{c2}\omega_{c2}\dot{g}(t)+\omega_{c2}^2 g(t) \text{ when } \bar{x}\geq g, \\ \ddot{\bar{x}}_o(t)+2\zeta_o\omega_o\dot{\bar{x}}_o(t)+\omega_o^2\bar{x}_o(t) = -\ddot{y}(t) \text{ when } \bar{x}<g. \end{aligned} \tag{2}$$

The new parameters used in Eqn. (2) are given as

$$\omega_o^2=\frac{k}{m}\ ,\ \zeta_o=\frac{c}{2m\omega_o},$$
$$\omega_{c1}^2=\frac{k}{\bar{m}}\ ,\ \zeta_{c1}=\frac{c}{2\bar{m}\omega_{c1}}\ ,\ \omega_{c2}^2=\frac{k^*}{\bar{m}}\ ,\ \zeta_{c2}=\frac{c^*}{2\bar{m}\omega_{c2}}.$$

The BAA method was developed for periodic excitation cases, and for simplicity this work will assume a harmonic excitation $y(t)=y_0\sin(\alpha t)$ in which y_0 is the amplitude of excitation and α is the excitation frequency. Next, dimensionless variables are introduced. The time related dimensionless variables are:

$$\tau_o=\omega_o t\ \ ,\ \rho_o=\frac{\alpha}{\omega_o},$$
$$\tau_c=\omega_{c1}t\ \ ,\ \rho_c=\frac{\alpha}{\omega_{c1}}\ \ ,\ \rho_c^*=\frac{\omega_{c1}}{\omega_{c2}}.$$

Using the dimensionless variables, Eqn. (2) can then be represented as:

$$\begin{aligned} \bar{x}_c''(\tau_c)+2(\zeta_{c1}+\zeta_{c2}\rho_c^*)\bar{x}_c'(\tau_c)+(1+\rho_c^{*2})\bar{x}(\tau_c) = \\ \rho_c^2 y_0\sin(\rho_c\tau_c)+2\zeta_{c2}\rho_c^* g'(\tau_c)+\rho_c^{*2}g(\tau_c) \text{ when } \bar{x}\geq g, \\ \bar{x}_o''(\tau_o)+2\zeta_o\bar{x}_o'(\tau_o)+\bar{x}_o(\tau_o) = \rho_o^2 y_0\sin(\rho_o\tau_o) \text{ when } \bar{x}<g, \end{aligned} \tag{3}$$

where the symbol $(')$ denotes differentiation with respect to the time variable τ. Note that due to the nature of the dimensionless variables chosen, $\tau_o\neq\tau_c$ and $\rho_o\neq\rho_c$ at a given excitation frequency α. To convert between the closed and open domains for analysis, the following conversions must be completed.

$$\tau_o=\tau_c\sqrt{\frac{\bar{m}}{m}}\ \text{ and }\ \rho_o=\rho_c\sqrt{\frac{m}{\bar{m}}}. \tag{4}$$

Lastly, the displacement related dimensionless variables are introduced

$$u=\frac{\bar{x}}{y_0}\ \text{ and }\ \delta=\frac{g}{y_0}. \tag{5}$$

These variables allow for the pre-computation of all responses independent of the base motion since $\bar{x}$ and g have been scaled by the input signal amplitude y_0. The final equation of motion can then be written as:

$$\begin{aligned} u_c''(\tau_c)+2(\zeta_{c1}+\zeta_{c2}\rho_c^*)u_c'(\tau_c)+(1+\rho_c^{*2})u(\tau_c) = \\ \rho_c^2\sin(\rho_c\tau_c)+2\zeta_{c2}\rho_c^*\delta'(\tau_c)+\rho_c^{*2}\delta(\tau_c) \text{ when } u\geq\delta, \\ u_o''(\tau_o)+2\zeta_o u_o'(\tau_o)+u_o(\tau_o) = \rho_o^2\sin(\rho_o\tau_o) \text{ when } u<\delta. \end{aligned} \tag{6}$$

System Dynamics

PWL oscillators have been studied extensively in recent decades [22, 23]. In order to effectively predict the dynamic response of these systems at various gap sizes, the BAA method is used to find the solution of Eqn. (6). The main idea of the BAA method is that one vibration cycle is the coupled response of the closed and open states. This method also assumes that the vibration cycle has only one interval in the open state and one interval in the closed state. This gives an overall period $T=T_o+T_c$ where T_o is the time interval in the open state and T_c is the time interval in the closed state. After setting $\delta'(\tau_c)=0$, the coordinates of the system in the closed and open states can be represented by a combination of the linear steady-state and transient responses,

$$\begin{aligned} u_c(\tau_c) =& e^{-\bar{\zeta}\bar{\rho}\tau_c}a_c\sin(\sqrt{1-\bar{\zeta}^2}\bar{\rho}\tau_c+\phi_c) \\ &+\frac{(\rho_c/\bar{\rho})^2\sin(\rho_c\tau_c-\theta_c+\Psi)}{\sqrt{[1-(\rho_c/\bar{\rho})^2]^2+(2\bar{\zeta}\rho_c/\bar{\rho})^2}}+\delta(\frac{\rho_c^{*2}}{1+\rho_c^{*2}}), \\ u_o(\tau_o) =& e^{-\zeta_o\tau_o}a_o\sin(\sqrt{1-\zeta_o^2}\tau_o+\phi_o) \\ &+\frac{\rho_o^2\sin(\rho_o\tau_o-\theta_o+\Psi)}{\sqrt{(1-\rho_o^2)^2+(2\zeta_o\rho_o)^2}}. \end{aligned} \tag{7}$$

where $\bar{\rho}=\sqrt{1+\rho_c^{*2}}$, $\bar{\zeta}=(\zeta_{c1}+\zeta_{c2}\rho_c^*)/\sqrt{1+\rho_c^{*2}}$, $\theta_c=\tan^{-1}(2\bar{\zeta}\rho_c\bar{\rho}/(\bar{\rho}^2+\rho_c^2))$, and $\theta_o=\tan^{-1}(2\zeta_o\rho_o/(1-\rho_o^2))$; a_c

and a_o are scalar coefficients representing the amplitude of the transient response; ϕ_c and ϕ_o are phase angles of the linear transient responses; and the angle Ψ represents the phase difference between the excitation and steady state response that results from the piecewise linear nonlinearity.. To solve for the unknowns in Eqn. (7), a nonlinear optimization solver is used to minimize the residual of the following compatibility conditions:

$$\begin{aligned} &u_c(0) = \delta, \\ &u_c(T_c) = \delta, \\ &u_o(T_c) = \delta, \\ &u_o(T_c + T_o) = \delta, \\ &u_c'(T_c) = u_o'(T_c), \\ &u_c'(0) = u_o'(T_c + T_o). \end{aligned} \tag{8}$$

In Eqn. (8), the first four conditions are the displacement compatibility conditions at the transition from the closed to open state and vice versa. The remaining two equations represent the velocity compatibility at the transition between states. Note that the time T_c is also an unknown in Eqn. (8) since it cannot be predetermined. The function 'lsqnonlin' in Matlab [24] was used to solve for this parameter as well as the other unknowns. Once these values are determined, the entire vibration cycle for the chosen gap-size can be constructed. A detailed overview of how the BAA method is used to construct the response of the idealized nondimensionalized system has previously been published [17].

Electromagnetic Model

In order to predict the power output of the harvester, a computational model of the electromagnetic induction was also added to the model. In the preliminary steps of this investigation, an electromagnetic transducer was chosen as the method of energy conversion. Another method that researchers commonly use is piezoelectric transduction, which generates a charge in response to applied mechanical stress. These usually take the form of a cantilevered beam made of a piezoelectric material. While these devices are suited for certain applications including small-scale devices experiencing small deflections, the intended application of a bench-top system with large motions led to the selection of the electromagnetic transduction. Electromagnetic methods are also more commonly used in large scale harvesting including wave power generation [25].

In the physical system, a magnet is added to the oscillating mass which moves through a coil. Faraday's law states that the induced electromotive force (emf) due to the relative motion of the magnet and coil is given by

$$emf = -\frac{d\psi}{dt} = -\frac{d\psi}{dz}\left|\frac{dz}{dt}\right|, \tag{9}$$

where ψ denotes the total magnetic flux through the coil turns. The magnetic flux through a single coil [26] turn is then calculated as

$$\psi = \frac{\mu_0 M}{2}\left[\frac{1}{\sqrt{r^2+z^2}} - \frac{z^2}{(r^2+z^2)^{3/2}}\right]. \tag{10}$$

Differentiating with respect to z then gives

$$\frac{d\psi}{dz} = \frac{\mu_0 M}{2}\left[\frac{2*z^3}{(r^2+z^2)^{5/2}} - \frac{3z}{(r^2+z^2)^{3/2}}\right]. \tag{11}$$

Equation (11) gives the flux change through one coil of distance z from the dipole center of radius r, μ_0 denotes the permeability of free space, and M denotes the magnetic moment of the magnet used. The magnetic flux change through the entire coil with N turns of length l is finally expressed as

$$\begin{aligned} \frac{d\psi}{dz} = \frac{\mu_0 M}{2}\sum_{n=-N/2}^{n=N/2} z_n\left[\frac{2*z_n^2}{(r^2+z_n^2)^{5/2}} - \frac{3}{(r^2+z_n^2)^{3/2}}\right], \\ \text{where } z_n = z + n\left(\frac{l}{N-1}\right). \end{aligned} \tag{12}$$

With the calculated emf at each point in time, the root mean squared voltage value and resistance R is then used to determine the average power (P_{avg}) generated by the harvester as given in Eqn. (13)

$$P_{avg} = \frac{v_{rms}^2}{R}. \tag{13}$$

Experimental Setup

In this section, the experimental setup of a PWL nonlinear oscillator with an adjustable gap size is presented. In this investigation, an oscillating linear mass-spring system is coming into intermittent contact with a mechanical stopper. The experimental setup used can be seen in Fig. 2. The system is comprised of a mass on a linear guide rail attached to the base of the system by extension springs. At one end of the linear guide rail, a linear actuator (P8, Actuonix) with a mechanical stopper attached to its end is placed with its shaft collinear to the motion of the mass. By adjusting the position of the actuator, the gap size between the mass and stopper can be changed, and hence the resonance frequency of the PWL system can be tuned to different

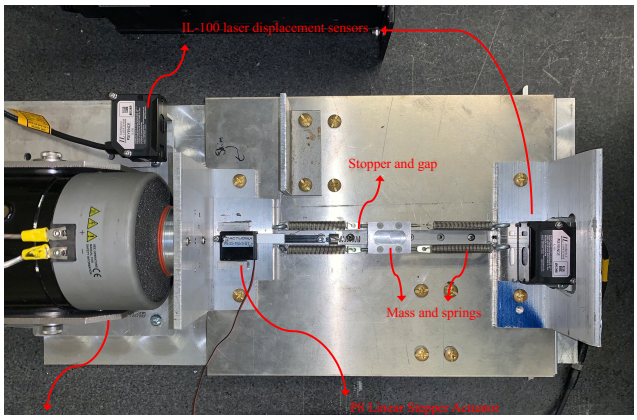

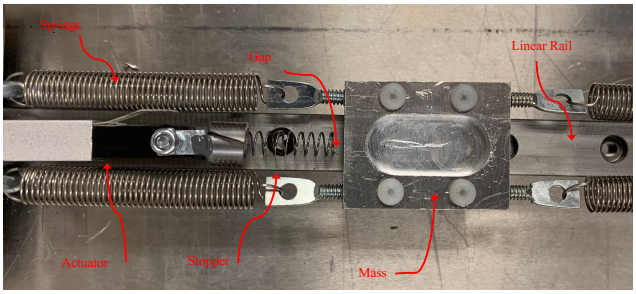

(b)

FIGURE 2: (a): Experimental setup top-view. (b): Close-up view of mass and stopper.

frequencies. The surface containing the rail, mass, and actuator is connected to a horizontally mounted electrodynamic shaker (ET-126B, Labworks) that creates a base excitation motion in the direction of the linear rail. To monitor the system coordinates, laser displacement sensors (IL-100, Keyence) are utilized. One sensor is mounted on the base to capture the mass motion relative the base ($\bar{x}$) and one sensor is mounted on the vibration table to capture the base motion (y).

Parameter Identification

Before analyzing the PWL system, experiments were conducted to characterize the linear single DOF system. By studying the forced response of this system for different cases, the parameters in Fig. 1 of the oscillator (i.e., m, c, and k) were identified. This process was necessary for the investigation since in a physical system the inertia of the springs cannot be neglected, and the damping values needed to be experimentally determined.

The single DOF system was subjected to a sinusoidal frequency up-sweep while the motion of the base and mass were monitored. The displacement transmissibility at each frequency

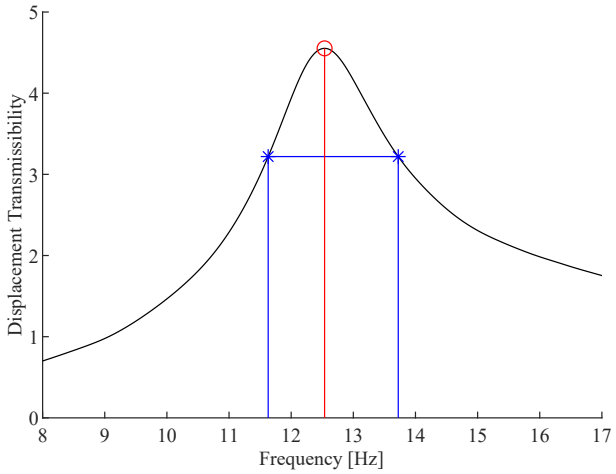

FIGURE 3: Displacement Transmissibility of 1 DOF system with half power points indicated by blue star and resonant peak indicated by red circle.

point of the sweep was then calculated giving a displacement transmissibility curve and resonant frequency, which is shown in Fig. 3. From the transmissibility curve, the damping ratio ζ can be estimated using the half-power bandwidth method given in Eqn. (14)

$$\zeta = \frac{f_2 - f_1}{2f_{peak}}, \tag{14}$$

where f_1 and f_2 are the frequencies at the half-power points and f_{peak} is the resonanace frequency of the system. The half power points and resonance frequency are noted in Fig. 3 for one case.

With the damping ratio and resonant frequency calculated, the natural frequency of the system can then be determined. Using the measured mass, the spring stiffness k and damping c can then be calculated using fundamental equations of damped linear oscillators.

This process was conducted with two different mass values, giving two sets of m, k, and c. As the mass was the only parameter changed between the cases, the values of k and c should be consistent between the two cases. This was not found to be true when the inertia in the springs was not accounted for in the mass term. By optimizing the mass addition from the springs, the values of k and c determined in the two cases converge to nearly the same value.

In the optimization, one third of the spring mass was chosen as a reference value for the mass contribution as this is the effective mass of an ideal spring. The necessary parameters were then calculated for mass contributions ranging from 0 to 2.5 times the

TABLE 1: Estimated system parameters.

Case	m [kg]	k [N/m]	c [N s/m]
1	0.0857	436.80	0.8836
2	0.0686	430.83	0.8583

ideal effective mass. The iteration most consistent between the two cases was then chosen for the remainder of the analysis. The parameters identified for the nominal system are given in Tab. 1.

Since the optimization did not converge to single values of stiffness and damping, the average values of $k = 433.82$ N/m and $c = .87095$ N s/m were assumed to be the system parameters for the analysis. The same process was conducted for the stopper characterization with the system in the closed state for the entire vibration cycle. This process gave $m^* = 1.75g$, $k^* = 182.104$ N/m, and $c^* = 0.695$ N s/m as the assumed parameter values.

PHYSICAL INVESTIGATION

In this section, the bench-top system is tested at various excitation conditions with the gap size set to the precomputed position for maximum transmissibility. These experimental results are then compared to the simulation response at the same frequency and gap size. Note that the gap size used in the physical testing was set to 87% of the computed value. This is to ensure that the system maintains intermittent contact and avoids the undesired jump phenomenon due to any excitation signal perturbations [17]. The system parameters were first converted into the dimensionless variables used in the computational tool. These calculated parameters are given in Tab. 2.

Inputting these values in the computational tool, the maximum response envelope and precomputed gap size over the frequency range bounded by the linear responses of the closed and open states is constructed and shown in Fig. 4. Note: the response envelope of the device when the gap size is set to 87% of the optimal δ_r value is also plotted in black.

For the physical validation, four arbitrary frequency points were compared to the results of the numerical tool. Two of the chosen excitation frequencies occur where the optimal gap size

TABLE 2: Dimensionless variable values.

Variable	Value	Variable	Value
ω_{c1}	71.14	ω_{c2}	46.09
ζ_{c1}	0.07137	ζ_{c2}	0.08859
ω_o	71.15	ζ_o	0.07142
ρ_c*	0.6479		

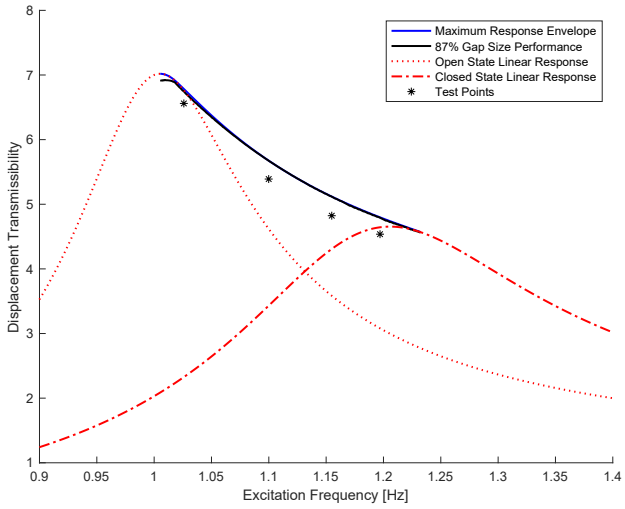

(a)

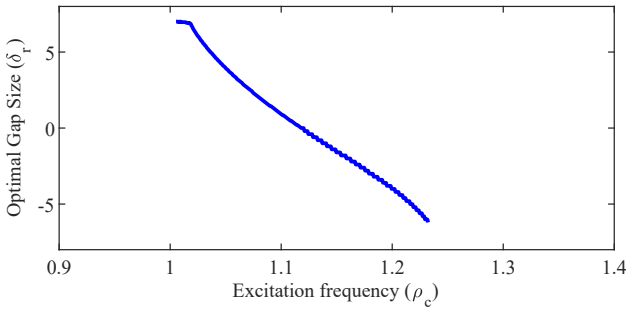

(b)

FIGURE 4: (a): Response envelopes and linear responses plotted with test points (*) (b): Precomputed optimal gap sizes.

(δ_r) is positive and two occur where the optimal gap size is negative. The four chosen frequency values can be seen in Tab. 3 with the experimental results. In this work, u_{comp} is used to denote the maximum transmissibility given by the numerical tool and u_{exp} denotes the experimentally calculated transmissibility. After converting the dimensionless parameters to the physical dimensioned form, the system was adjusted to 87% of δ_r and excited with sinusoidal motion until it reached steady-state. The motion of the mass and base were then measured and the experimental transmissibility was calculated.

Starting with the lowest frequency value, it is shown that the measured transmissibility of the base motion deviated from the expected value from the simulation by 3.32%. The process was then repeated for the next frequency value which gave an error between expected and measured transmissibility of 5.39%. The next two frequency values selected occurred where the optimal gap size was computed to be negative. The results from the

TABLE 3: Experimental results.

ρ_c	δ_r	u_{comp}	Frequency [Hz]	g [mm]	u_{exp}	Error [%]
1.026	5.956	6.785				
1.100	0.9207	5.675				
1.155	-1.752	5.119				
1.197	-3.754	4.799				

Frequency [Hz]	g [mm]	u_{comp}
11.62	21.6	6.785
12.45	3.40	5.675
13.08	4.03	5.119
13.55	7.88	4.799

third frequency value showed an error of 5.79% and the last frequency point gave an error of 5.61% from expected transmissibility. These results show that the error from the expected result ranged from 3% to 6% with an average error of 5.03%. The lowest error of 3.32% occurred at the largest gap size of 21.6 mm. A larger gap size coincides with a majority of the entire vibration period in the open state ($T_o > T_c$). The error then rose with decreased gap size or increased T_c. The lower error in the large gap case can most likely be attributed to an effective linear single DOF model, but a less effective PWL model due to certain assumptions made in the BAA method.

Although there was more error in the states with lower gap values, there is some error present in all four cases. This may suggest that the model and estimated parameters do not fully capture the dynamics of the system. This can most likely be attributed to other assumptions of the model including a linear spring rate and a simple viscous damping model versus one that accounts for Coulomb friction (e.g., between the moving mass and linear guide rail). Nevertheless, the simple model does capture the dynamics quite well. In the investigation, the performance of the harvester is shown to perform as effectively as a linear harvester at resonance. Figure 4a summarizes the results from the four frequency points and compares them to computational results.

Figure 4a shows that the method does an adequate job of capturing the expected dynamics of the PWL oscillator and the potential of an active control strategy for the gap size to tune the harvester to the excitation frequency.

Experiments were also conducted to test the electromechanical model by including an electromagnetic transducer into the experimental setup. The transducer added to the system consists of a coil wound around the mass's axis of motion and a magnet added to the carriage with its poles aligned with the rail. A model of the transducer can be seen in Fig. 5. The mechanical system creates relative motion between the magnet and coil which is amplified by the PWL system. This relative motion causes a flux variation in the coil turns which in turn generates an induced electromotive force (emf). This coil was placed in parallel with a load resistor, where the induced voltage is measured.

The parameters of the transducer used in this work are shown in Tab. 4. With the parameters identified, the system was tested at three stationary excitations with constant frequency. The power generated throughout the trial was monitored by

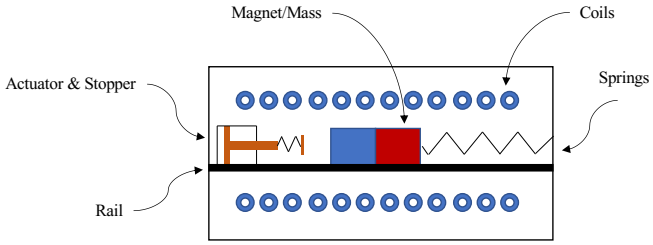

FIGURE 5: Energy harvester model.

the voltage across the load resistor while the displacement was tracked using the laser displacement sensors. The displacement transmissibility and average power generation are then compared to the simulation results. Table 5 summarizes the results of the investigation. Note that the measured amplitude of the mass motion was used for the power generation simulation to test the accuracy of the model.

In the experiment, it was shown that the transmissibility errors fell in a similar range as discussed previously. As for the electrical generation, the experimental and computational results showed similar agreement in average power. While there was error present, these results show that the electromagnetic model also did an adequate job of capturing the system performance. The error in these results can most likely be attributed to assumptions made in the model about the magnetic field generated by the magnet. The model used did not account for the influence of ferromagnetic conductors near the magnet which can influence the field. While an attempt was made to minimize the amount of ferromagnetic material in the vicinity of the transducer, there were still components in the setup that could have influenced this field.

TABLE 4: Transducer Parameters

Coil diameter [m]	0.0762	Resistance [Ω]	220
Magnetic moment [A m^2]	15.363	Coil length [m]	0.053
Number of coil turns	15		

TABLE 5: Energy generation results.

			P_{avg} [μW]		
Frequency [Hz]	g [mm]	Transmissibility Error [%]	Experiment	Computational	Error [%]
13.07	13.7	3.22	32.70	31.50	3.67
13.71	1.60	2.54	23.40	24.80	5.98
14.45	-6.30	4.59	17.07	17.79	4.22

CONCLUSION

In this work, the performance of a PWL energy harvester with a controllable gap was studied for the first time in a physical system. In this system, the resonant frequency of the device was tuned to match the excitation frequency by setting the gap to the precomputed optimal position. Modifications to the computational method are also presented to account for parameters not considered in the underlying work as well as an energy generation model. The investigation showed that the results measured from the physical system followed the expected behavior from the computational tool, although as expected there was some error present in the computational prediction when compared to the physical nonlinear system. The investigation also showed the electrical generation model was in good agreement with the experimental results.

Future studies of this system should include analysis of the net power gained from the process. In this work, the energy required to drive the actuator and power the sensors was not compared to the generated power. This is because the current system was not optimized for maximum transduction and minimal power use. With the system now validated, future work needs to include transducer and sensor optimization to ensure a net power gain.

To further verify the new PWL energy harvester idea, additional studies need to be conducted that incorporate the active control method. The stopper must currently be manually set to its optimal position, making sweeping and changing excitation conditions difficult to study. An automatic control system would allow for the physical system and computational tool to be tested at many different excitation conditions including sweeping or arbitrarily changing frequency and amplitude.

Additionally, to improve the energy generation and overall displacement amplification, the experimental setup should be modified to reduce the damping in the system. By reducing the overall damping in the system, the effectiveness of the harvester and control system will be increased compared to the current system, and will better demonstrate the effectiveness of the system compared to traditional methods. The last proposed improvement is to the control system for the harvester. Currently, the process assumes that the excitation signal is measured to compute the optimal gap size. To simplify the design and reduce the number of required sensors, only the system response will be measured. Using the response information along with the other known system parameters, the excitation signal can be determined. This reduction in complexity allows for less of the generated power to be used in the control process and sensing equipment, therefore harvesting more power for external use.

ACKNOWLEDGMENT

This paper is based on work supported by the National Science Foundation under Grant No. 1902408, program manager Dr. Harry Dankowicz. Any opinions, findings, and conclusions or recommendations expressed in this paper are those of the authors and do not necessarily reflect the views of the National Science Foundation.

REFERENCES

[1] Paradiso, J. A., Paradiso, J. A., and Starner, T., 2005. "Energy scavenging for mobile and wireless electronics". *IEEE pervasive computing,* ***4***(1), Jan., pp. 18–27.

[2] Daqaq, M. F., Masana, R., Erturk, A., and Quinn, D. D., 2014. "On the role of nonlinearities in vibratory energy harvesting: A critical review and discussion". *Applied mechanics reviews,* ***66***(4), July.

[3] Khan, F. U., and Iqbal, M., 2016. "Electromagnetic-based bridge energy harvester using traffic-induced bridge's vibrations and ambient wind". In 2016 International Conference on Intelligent Systems Engineering (ICISE), pp. 380–385.

[4] Nabavi, S. F., Farshidianfar, A., and Afsharfard, A., 2018. "Novel piezoelectric-based ocean wave energy harvesting from offshore buoys". *Applied Ocean Research,* ***76***, pp. 174–183.

[5] Viet, N., Xie, X., Liew, K., Banthia, N., and Wang, Q., 2016. "Energy harvesting from ocean waves by a floating energy harvester". *Energy,* ***112***, pp. 1219–1226.

[6] Gunn, K., and Stock-Williams, C., 2012. "Quantifying the global wave power resource". *Renewable Energy,* ***44***, Aug., pp. 296–304.

[7] Aderinto, T., and Li, H., 2018. "Ocean wave energy converters: Status and challenges". *Energies,* ***11***(5), June.

[8] Poulin, G., Sarraute, E., and Costa, F., 2004. "Generation of electrical energy for portable devices". *Sensors and actuators. A. Physical.,* ***116***(3), Oct., pp. 461–471.

[9] Liu, J.-Q., Fang, H.-B., Xu, Z.-Y., Mao, X.-H., Shen, X.-C., Chen, D., Liao, H., and Cai, B.-C., 2008. "A mems-

based piezoelectric power generator array for vibration energy harvesting". *Microelectronics Journal,* ***39***(5), Sept., pp. 802–806.

[10] Marinkovic, B., and Koser, H., 2012. "Demonstration of wide bandwidth energy harvesting from vibrations". *Smart Materials and Structures,* ***21***(6), May, p. 065006.

[11] Wei, C., and Jing, X., 2017. "A comprehensive review on vibration energy harvesting: Modelling and realization". *Renewable sustainable energy reviews,* ***74***, July, pp. 1–18.

[12] Tran, N., Ghayesh, M. H., and Arjomandi, M., 2018. "Ambient vibration energy harvesters: A review on nonlinear techniques for performance enhancement". *International journal of engineering science,* ***127***, Apr., pp. 162–185.

[13] Mann, B. P., and Sims, N. D., 2009. "Energy harvesting from the nonlinear oscillations of magnetic levitatio". *Journal of Sound and Vibration,* ***319***(1-2), Feb., pp. 515–530.

[14] Liu, H., Lee, C., Kobayashi, T., Tay, C. J., and Quan, C., 2012. "Investigation of a mems piezoelectric energy harvester system with a frequency-widened-bandwidth mechanism introduced by mechanical stoppers". *Smart materials and structures,* ***21***(3), Mar.

[15] Wu, Y., Badel, A., Formosa, F., Liu, W., and Agbossou, A., 2014. "Nonlinear vibration energy harvesting device integrating mechanical stoppers used as synchronous mechanical switches". *Journal of Intelligent Material Systems and Structures,* ***25***(14), pp. 1658–1663.

[16] Liu, S., Cheng, Q., Zhao, D., and Feng, L., 2016. "Theoretical modeling and analysis of two-degree-of-freedom piezoelectric energy harvester with stopper". *Sensors and Actuators A: Physical,* ***245***, pp. 97–105.

[17] Tien, M.-H., and D'Souza, K., 2020. "Method for controlling vibration by exploiting piecewise-linear nonlinearity in energy harvesters". *Proceedings of the Royal Society. A, Mathematical, physical, and engineering sciences,* ***476***(2233), Nov.

[18] Tien, M.-H., and D'Souza, K., 2017. "A generalized bilinear amplitude and frequency approximation for piecewise-linear nonlinear systems with gaps or prestress". *Nonlinear dynamics,* ***88***(4), June, pp. 2403–2416.

[19] Tien, M.-H., Hu, T., and D'Souza, K., 2018. "Generalized bilinear amplitude approximation and X-Xr for modeling cyclically symmetric structures with cracks". *J. Vib. Acoust,* ***140***, pp. 041012–10.

[20] Tien, M.-H., Hu, T., and D'Souza, K., 2019. "Statistical analysis of the nonlinear response of bladed disks with mistuning and cracks". *AIAA Journal,* ***57***(11), July, pp. 4966–4977.

[21] Tien, M.-H., D'Souza, K., and Lu, M., 2022. "Efficient analysis of piecewise-linear nonlinear systems modeled using general state-space representations". *Journal of Computational and Nonlinear Dynamics*.

[22] Shaw, S., and Holmes, P., 1983. "A periodically forced piecewise linear oscillator". *Journal of Sound and Vibration,* ***90***(1), pp. 129–155.

[23] Natsiavas, S., 1990. "On the dynamics of oscillators with bi-linear damping and stiffness". *International Journal of Non-Linear Mechanics,* ***25***(5), pp. 535–554.

[24] MATLAB, 2021. *version 9.10.0 (R2021a)*. The MathWorks, Natick, Massachusetts.

[25] Zuo, L., and Tang, X., 2013. "Large-scale vibration energy harvesting". *Journal of Intelligent Material Systems and Structures,* ***24***(11), pp. 1405–1430.

[26] Chow, T., 2006. *Introduction to Electromagnetic Theory: A Modern Perspective*. Jones and Bartlett Publishers.

[27] Tang, X., and Zuo, L., 2009. "Towards meso and macro scale energy harvesting of vibration". *ASME International Mechanical Engineering Congress and Exposition, Proceedings,* ***10***, 01.

[28] Blystad, L.-C. J., and Halvorsen, E., 2011. "A piezoelectric energy harvester with a mechanical end stop on". *Microsystem Technologies,* ***17***(4), pp. 505–511.

[29] Challa, V. R., Prasad, M. G., and Fisher, F. T., 2008. "Evaluation of coupled piezoelectric and electromagnetic technique for vibration energy harvesting". In Health Monitoring of Structural and Biological Systems 2008, T. Kundu, ed., Vol. 6935, International Society for Optics and Photonics, SPIE, pp. 588 – 597.

[30] Yuanyuan, F., Yingjun, S., Man, L., Shangguang, W., and Zujun, D., 2016. "Modeling and experimental verification of an electromagnetic and piezoelectric hybrid energy harvester". *Journal of Engineering and Technological Sciences,* ***48***(5), pp. 614–630.

[31] Li, H., Tian, C., and Deng, Z. D., 2014. "Energy harvesting from low frequency applications using piezoelectric materials". *Applied Physics Reviews,* ***1***(4), p. 041301.

[32] Shadoufa, M., Mahmoud, M., Ghoneima, M., and Dessouky, M., 2016. "Optimization of the output power of a frequency-up conversion piezoelectric energy harvester". In 2016 IEEE 59th International Midwest Symposium on Circuits and Systems (MWSCAS), pp. 1–4.

[33] Abedini, A., and Wang, F., 2019. "Energy harvesting of a frequency up-conversion piezoelectric harvester with controlled impact". *The European Physical Journal Special Topics,* ***228***, July, pp. 1459–1474.

[34] Noguchi, K., Saito, A., Tien, M., and D'Souza, K., 2022. "Bilinear systems with initial gaps involving inelastic collision: Forced response experiments and simulations". *Journal of Vibration, Acoustics, Stress, and Reliability in Design,* ***144***(2), Apr.